Polymer 50 (2009) 4293–4298

Contents lists available at ScienceDirect

Polymer

journal homepage: www.elsevier.com/locate/polymer

Preparation of Ni-*g*-polymer core–shell nanoparticles by surface-initiated atom transfer radical polymerization

Renxu Chen [a], Shane Maclaughlin [c], Gianluigi Botton [b], Shiping Zhu [a,b,*]

[a] Department of Chemical Engineering, McMaster University, Hamilton, Ontario, Canada L8S 4L7
[b] Department of Materials Science and Engineering, McMaster University, Hamilton, Ontario, Canada L8S 4L7
[c] Research and Development, Dofasco Inc., Hamilton, Ontario, Canada L8N 3J5

ARTICLE INFO

Article history:
Received 22 May 2009
Received in revised form
6 July 2009
Accepted 8 July 2009
Available online 14 July 2009

Keywords:
Atom transfer radical polymerization (ATRP)
Polymer composite materials
Ni nanoparticles

ABSTRACT

Surface-initiated atom transfer radical polymerization (si-ATRP) technique was successfully employed to modify Ni nanoparticles with polymer shells. ATRP initiators were covalently bonded onto Ni nanoparticle surfaces by a combination of ligand exchange and condensation reactions. Various kinds of polymers including poly(methyl methacrylate) (PMMA) and poly(*n*-isopropylacrylamide) (PNIPAM) were grafted from the immobilized initiators. The grated polymer shells gave Ni nanoparticles exceptionally good dispersion and stability in solvents. Fourier transform infrared (FT-IR) spectroscopy, thermogravimetric analysis (TGA) and transmission electron spectroscopy (TEM) were employed to confirm the grafting and to characterize the nanoparticle core–shell structure. Gel permeation chromatography (GPC) studies of cleaved polymer chains revealed that the grafting polymerization was well controlled. The magnetic properties of Ni-*g*-polymer nanoparticles were also studied.

1. Introduction

In recent years, because of the unique magnetic properties of nanocrystalline metallic nanoparticles such as Fe, Co and Ni, considerable attention has been devoted to the synthesis of these materials. In particular, Ni nanoparticles have received great interest for their potential applications in many diverse fields, including magnetic recording media, biomedical materials, catalysis, and electro-conductive materials. Numerous different physical and chemical preparative routes have been developed to synthesize Ni nanoparticles, such as pyrolysis [1], sputtering [2], microemulsion [3,4], aqueous [5,6] and nonaqueous [7,8,9] chemical reduction, sonochemical deposition [10], and polyol methods [11].

Because of the anisotropic dipolar attraction, Ni nanoparticles have strong tendency to aggregate into large clusters, thus lose their specific magnetic properties associated with the single-domain nanostructures. This greatly limits the uses of Ni nanoparticles in various applications. In order to overcome this problem, it is essential to do some modification work on Ni nanoparticle surface to prevent aggregation. In most preparation methods of Ni nanoparticles, capping agents like long chain alkyl acids, amines and phosphates were always applied to control growth of nanoparticles; and at the same time, to prevent them from aggregation.

Compared to small molecular capping agents, polymeric shells have their unique advantages. Because of flexibility in control of polymer composition and functionality, polymer shells are not only able to protect nanoparticles from aggregation, but also readily endow nanoparticles with interesting functionalities. Among many approaches for coating nanoparticles with polymer shells, surface-initiated polymerization techniques have recently become very popular choices, especially surface-initiated atom transfer radical polymerization (si-ATRP). By this method, polymer chains are *in situ* grafted from initiator molecules previously immobilized onto nanoparticle surfaces. The most significant advantage of this "grafting from" method is its ability to produce dense polymer brushes, with grafting densities ranged from 0.1 to 0.7 chains/nm^2. Moreover, ATRP is a well-established controlled radical polymerization technique and can offer good control over polymer molecular weight, and thus polymeric shell thickness, allowing preparation of polymer shells with low polydispersities.

Although si-ATRP has been employed to graft polymers from various nanoparticles, such as SiO_2 [12,13], Au [14], $MnFe_2O_4$ [15], etc, no successful experiments have been reported on modification of nanocrystalline metallic nanoparticles. Unlike other types of materials, metal surfaces are highly reactive in electrochemical and acid/base reactions that complicate ATRP reactions. Red-ox deactivation of

* Corresponding author. Department of Chemical Engineering, McMaster University, Hamilton, Ontario, Canada L8S 4L7. Tel.: +1 905 525 1940; fax: +1 905 521 1350.
E-mail address: zhuship@mcmaster.ca (S. Zhu).

0032-3861/$ – see front matter © 2009 Elsevier Ltd. All rights reserved.
doi:10.1016/j.polymer.2009.07.012

ATRP catalyst is a particular risk. In our previous study [16], using triethoxysilane-based initiator and iron catalyst, we succeeded in grafting polymer brushes from flat Ni and Cu surfaces. In this paper, we report the first successful study on surface modification of pristine Ni nanoparticles by si-ATRP. A combination of ligand exchange and condensation reaction was employed to covalently immobilize triethoxysilane-based ATRP initiators onto Ni nanoparticle surface. Various types of polymers, like poly(methyl methacrylate) (PMMA) and poly(*n*-isopropylacrylamide) (PNIPAM), were grafted *in situ* from the immobilized initiators. After polymer grafting, both dispersion and stability of the Ni nanoparticles in solvents were greatly improved. The grafted polymer shells were very effective to prevent the Ni nanoparticles from aggregation. The improved dispersion and stability, as well as good compatibility with polymer matrices, are of great benefit to preparation of high quality Ni nanoparticle/polymer composite materials.

2. Experimental

2.1. Materials

Nickel acetylacetonate [Ni(acac)$_2$] (95%), hexadecylamine (HDA) (98%), trioctylphosphine oxide (TPPO) (99%), sodium borohydride (99%), *o*-dichlorobenzene (anhydrous, 99%), acetic acid (≥99.7%), 3-aminopropyltriethoxysilane (99%), 2-bromoisobutyryl bromide (98%), triethylamine (>99%), iron(II) bromide (98%), iron(III) bromide (98%), triphenylphosphine (TPP) (99%), toluene (anhydrous,99.8%), *N*,*N*-dimethylformamide (DMF) (anhydrous, 99.8%), *n*-isopropylacrylamide (NIPAM) (97%) were purchased from Aldrich and were used as received. Methyl methacrylate (MMA) (99%) was purchased from Aldrich and distilled over CaH_2 under vacuum, then stored at −15 °C before use. Ethanol (anhydrous), hexane (reagent), chloroform (reagent), dichloromethane (reagent), ethyl acetate (reagent), tetrahydrofuran (THF) (HPLC) and hydrochloric acid solution (37 wt.-%) were obtained from Caledon Laboratories Ltd. and used as received. Deionized (DI) water with a resistivity of 18 MΩ cm was prepared from a Millipore Milli-Q filtration system. Ultra-high-purity-grade argon was used in this study.

2.2. Synthesis of Ni nanoparticles

Ni nanoparticles were synthesized following the published procedure [17]. The synthesis was conducted using a standard airless technology. 0.2 g of Ni(acac)$_2$ was dissolved in 5 mL *o*-dichlorobenzene at 100 °C, and the solution was quickly injected into a mixture containing 40 mL dichlorobenzene, 1.5 g TOPO, 1.5 g HDA, and 0.15 g sodium borohydride at 140 °C during vigorously stirring. The mixture was quickly heated to 180 °C and stirred for 30 min under Ar atmosphere. It was then cooled to room temperature. 100 mL ethanol was added to precipitate Ni nanoparticles. The nanoparticles were separated by centrifugation (3500 rpm, 1 h) and dried in vacuum. The dried nanoparticles were redispersed into toluene and re-precipitated in ethanol. The cycle was repeated for three times to remove excess ligands. Finally, Ni nanoparticles were dispersed in toluene with a concentration of 10 mg/mL.

2.3. Immobilization of initiators

The surface-attachable initiator was synthesized following the same procedure as in our previous work [16]. The initiator was immobilized onto Ni nanoparticles as follows: 0.25 mL initiator, 50 μL acetic acid and 50 mL toluene based Ni nanoparticle dispersion were mixed in a 100 mL round-bottom flask. The mixture was stirred at room temperature for 72 h under argon protection. 100 mL *n*-hexane was added into the mixture to precipitate the initiator-modified Ni nanoparticles. The nanoparticles were separated by centrifugation (3500 rpm, 1 h) and dried in vacuum. The dried nanoparticles were redispersed into toluene and re-precipitated by *n*-hexane. The wash cycle was repeated for five times to remove excess initiators. Finally, the initiator-modified Ni nanoparticles were dispersed in toluene with a concentration of 10 mg/mL.

2.4. Surface-initiated ATRP on Ni nanoparticle

The typical procedure for ATRP of MMA from Ni nanoparticle surface is as follows: 64.7 mg (0.300 mmol) $FeBr_2$, 8.9 mg (0.030 mmol) $FeBr_3$ and 259.6 mg (0.9900 mmol) triphenylphosphine were placed into a 25 mL flask containing a magnetic stir bar. The flask was deoxygenated through several evacuation/backfilling cycles of argon. 6.0 g (60 mmol) MMA and 6.0 g initiator-modified Ni nanoparticle dispersion in toluene were purged with Ar for 1 h before added into the flask containing iron catalyst via a double-tipped needle. The mixture was stirred intensively, degassed with argon for another 10 min, and put into an oil bath of 60 °C. After the desired reaction time was reached, the polymerization solution was taken out from the oil bath, diluted with 50 mL THF. The Ni-*g*-PMMA nanoparticles were collected by centrifugation (20,000 rpm, 1 h). The nanoparticles were repeatedly rinsed with large amount of THF to remove residual monomer and free polymer. Finally, the samples were dried in vacuum at 50 °C for 6 h. The polymerization of NIPAM was performed at 40 °C in DMF. After the reaction, the polymerization solution was diluted with methanol at a solution/methanol ratio of 1/4. The Ni-*g*-PNIPAM nanoparticles were also collected by centrifugation (20,000 rpm, 1 h), washed intensively with methanol and then dried in vacuum.

2.5. Cleavage of PMMA chains from Ni nanoparticles

Grafted PMMA brushes were cleaved from the Ni nanoparticle surfaces with the method described by Matsuno et al. [18]. Hydrochloric acid solution was used to dissolve the Ni nanoparticles. PMMA was extracted with chloroform. The chloroform was then removed under vacuum and PMMA was subjected to GPC measurement.

2.6. Characterization

Fourier transform infrared analysis was performed on a Bio-Rad FTS-40 FT-IR spectrometer. All samples were prepared as pellets using spectroscopic grade KBr in a Carver press at 15,000 psi. The spectra were scanned over the range 4000–400 cm^{-1} in the transmission mode, accumulating 16 scans at a resolution of 2 cm^{-1}. TEM was carried out on a Philips CM-12 transmission electron microscope. The samples were dispersed in appropriate solvents with ultrasonication for 2 min and then dropped onto the copper grid to dry. Magnetic studies were carried out using a Quantum Design MPMS SQUID magnetometer at 5 K and 298 K.

TGA was performed on using a Thermowaage STA409, at a scan rate of 10 °C/min, up to 800 °C in nitrogen atmosphere. The initiator density on nanoparticle surfaces and the grafting densities of polymer chains were calculated from the TGA results according to the following equation:

$$\text{Density}\left(\text{molecules}/\text{nm}^2\right) = \frac{W \times r \times N_A \times d_{Ni}}{M(1-W) \times 3 \times 10^{21}}$$

where W is the weight loss of sample, r is the radius of Ni nanoparticles, N_A is Avogadro's constant, d_{Ni} is the density of nickel (8.90 g/cm^3), and M is the polymer molecular weight.

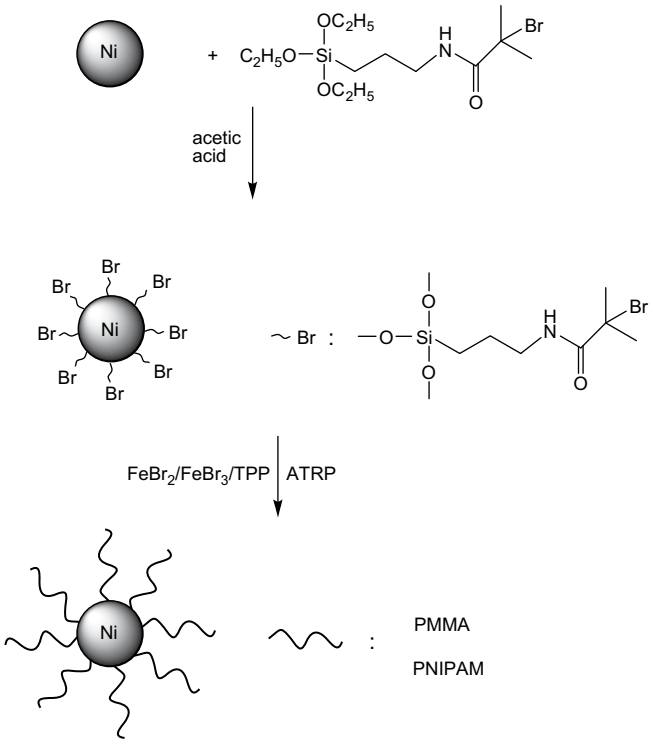

Scheme 1. Surface-initiated ATRP of polymers from Ni nanoparticle surface.

The molecular weights of PMMA were determined by gel permeation chromatography (GPC). A Waters 710 sample auto injector, 3 linear columns in series (Waters Styragel HR 5E, 2 Shodex KF-804L), a Waters 600 pump system and a 410 refractive index (RI) detector were used for the assays. The eluent (THF) was pumped through the system at a fixed flow rate of 1 mL/min. The columns and detector were heated to 30 °C and 35 °C, respectively. Narrow polystyrene samples were used as standards to generate the calibration curve. Data were recorded and manipulated using the Waters Millennium software package.

3. Result and discussion

3.1. Immobilization of initiator on Ni nanoparticle

Ligand exchange reaction is an effective way to modify nanoparticle surface with ATRP initiators. For metal oxide nanoparticles, carboxylic acid-based initiators are often used to replace the ligands on nanoparticle surfaces, followed by *in situ* polymerization. However, this method has a drawback. The carboxylate bond between polymer chain and nanoparticle surface is not strong enough to achieve a stable linkage. The polymer chains are readily dissociated from the nanoparticle surface through dynamic exchange with other competing ligands. Trialkoxysilane-containing ATRP initiators have already been proven effective for surface-initiated ATRP from many different substrates [16,19,20], including flat copper and nickel surfaces in our previous studies. The trialkoxysilane-type initiators can be immobilized onto metal surfaces with stable metal–O–Si bonds. The reaction is mild and does not present a risk of corrosion damage of reactive metal surfaces. Inspired by these advantages, we tried the same triethoxysilane-containing initiator in this work. A catalyst, such as acetic acid, was required in the initiator immobilization process. It can react with replaced amine ligand to accelerate the ligand exchange reaction. It could also accelerate the hydrolyzation of Si–$(OC_2H_5)_3$ groups to Si–$(OH)_3$ groups. The Si–$(OH)_3$ groups form hydrogen bonds with hydroxyl groups on metal surfaces, followed by condensation reactions to produce a very dense initiator layer covalently bonded to the metal surface by metal–O–Si bonds.

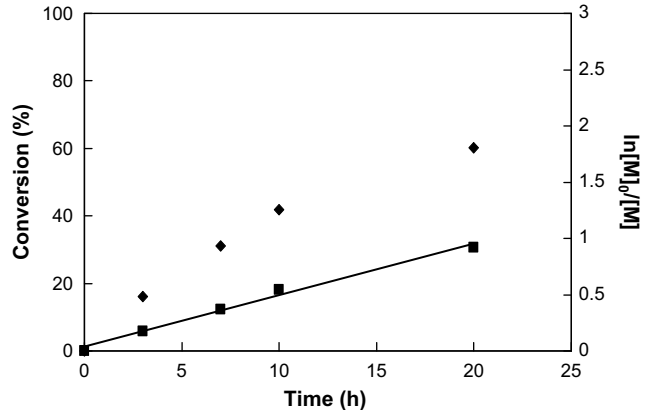

Fig. 1. Plot of $\ln([M]_0/[M])$ versus reaction time for the solution polymerization of MMA from Ni nanoparticles at 70 °C.

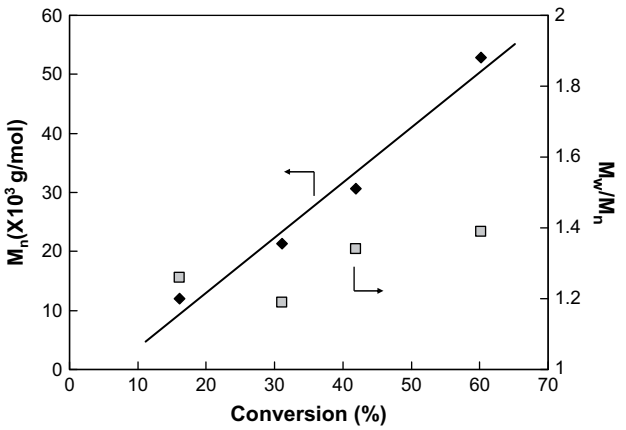

Fig. 2. Plot of M_n and polydispersity versus monomer conversion for the solution polymerization of MMA from Ni nanoparticles at 70 °C.

3.2. Surface-initiated ATRP on Ni nanoparticles

An iron catalyst system was chosen for the polymerization on nickel surface instead of copper catalyst because of the risk of nickel corrosion by Cu(II) catalyst (Scheme 1). MMA was first used as

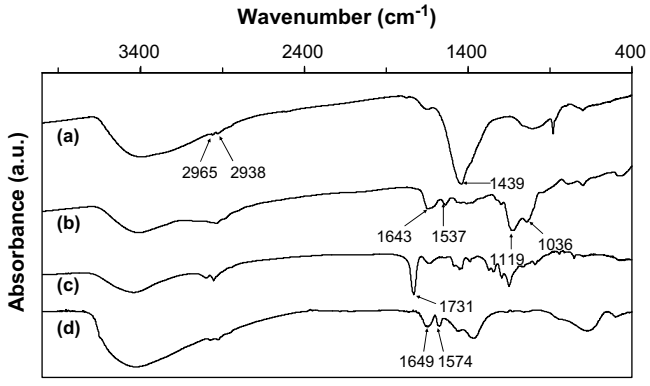

Fig. 3. FT-IR spectra of (a) pristine Ni nanoparticles; (b) Initiator coated Ni nanoparticles; (c) PMMA coated Ni nanoparticles; (d) PNIPAM coated Ni nanoparticles.

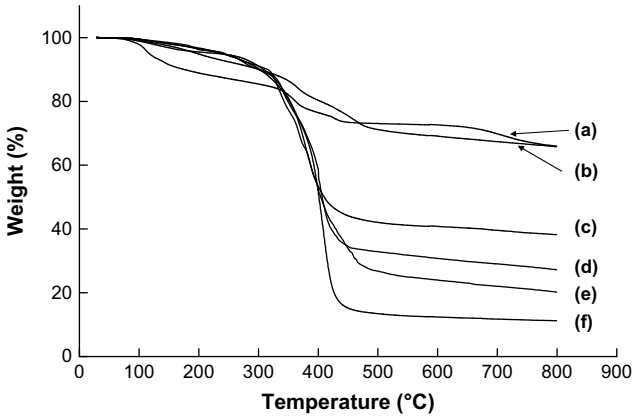

Fig. 4. TGA curves of (a) pristine Ni nanoparticles; (b) Initiator coated Ni nanoparticles and (c–f) PMMA coated Ni nanoparticles with polymerization time of 3, 7, 10 and 20 h, respectively.

a model monomer and was polymerized from Ni nanoparticle surface with added deactivator. In order to study the si-ATRP kinetics, hydrochloric acid was added to dissolve the nickel cores and "free" PMMA chains were released for GPC characterization. Fig. 1 shows the conversion profiles. A first-order kinetic plot of monomer conversion versus time was obtained. The grafted polymer chains were cleaved from the nanoparticles by dissolving the Ni core with hydrochloric acid (37 wt.-%) followed by the molecular weight measurement. Fig. 2 shows the molecular weight (M_n) and polydispersity index (M_w/M_n) of the cleaved PMMA polymers. The molecular weight increased linearly with the monomer conversion. For all the polymers, the polydispersity remained lower than 1.40, independent of the polymerization time. These results indicated that the grafting polymerization from Ni nanoparticle surface was well controlled by the ATRP technique.

Other than MMA, we also grafted other monomers with different functionalities using this ATRP technique. In grafting PNIPAM, more polar DMF, instead of toluene, was selected as the solvent for its good solubility of all the experimental components. FT-IR spectroscopy was employed to study the chemical structure of the core–shell Ni-*g*-polymer particles. Fig. 3(a) shows the FT-IR spectrum of pristine Ni nanoparticles. The absorption bands characteristic of the functional groups in alkyl chain surfactants, such as 2965 and 2938 cm^{-1} of the $-CH_3$ and $-CH_2$ groups, 1439 cm^{-1} of the alkane, were observed. After the initiator modification, the characteristic peaks of the N–C═O bond at 1643 cm^{-1} and 1537 cm^{-1} became apparent in Fig. 3(b). The peak at 1119 cm^{-1} and the neighboring peak at 1036 cm^{-1} were attributed to the Si–O–Ni and Si–O–Si vibrations, respectively. These results confirmed the formation of an initiator layer around the Ni nanoparticles. The FT-IR spectrum of Ni-*g*-PMMA is shown in Fig. 3(c). The characteristic peak of the O–C═O group of PMMA was found at 1731 cm^{-1}, which was not present in the spectrum of pristine Ni nanoparticles. The successful grafting of PNIPAM was also verified by FT-IR spectroscopy. The absorption bands centered at about 1649 cm^{-1} and 1574 cm^{-1} in Fig. 3(d) were attributed to the vibration of amide (N–C═O) groups.

Table 1
Weight loss and grafting density data of Ni nanoparticle samples.

Sample	Weight loss (%)	Grafting density (chains/nm^2)
Ni NPs	34.03	
Ni-initiator	34.23	26.7
Ni-*g*-PMMA (3 h)	61.76	1.20
Ni-*g*-PMMA (7 h)	72.76	1.13
Ni-*g*-PMMA (10 h)	79.82	1.15
Ni-*g*-PMMA (20 h)	88.76	1.32

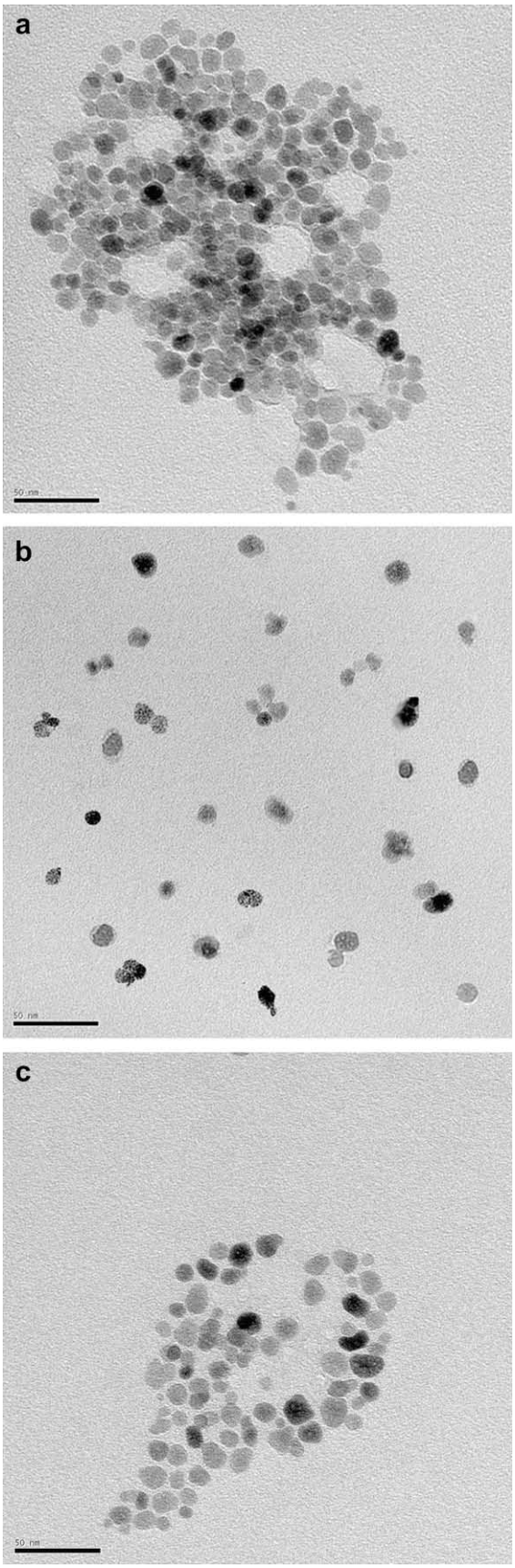

Fig. 5. TEM images of (a) pristine Ni nanoparticles in toluene; (b) PMMA coated Ni nanoparticles in toluene; (c) PNIPAM coated Ni nanoparticles in methanol. Scale bar: 50 nm.

Table 2
Magnetic characteristics of pristine Ni and Ni-*g*-PMMA nanoparticles.

Sample	Saturation magnetization at 5 K (emu/g)	Saturation magnetization at 298 K (emu/g)	Coercivity at 5 K (Oe)	Coercivity at 298 K (Oe)
Ni	32.7	31.1	410	0
Ni-*g*-PMMA (3 h)	12.1	11.7	382	0
Ni-*g*-PMMA (10 h)	6.4	6.2	389	0

TGA is an effective method to determine grafting densities of polymer chains anchored to inorganic nanoparticles. Fig. 4 shows the TGA curves. The weight losses and grafting densities for Ni-*g*-PMMA are summarized in Table 1. As shown in Fig. 4, the pristine Ni nanoparticles started to lose weight faster than other samples, which might be due to the weak bondings between ligand molecules and nanoparticle surface. The polymer content in the composite increased with the polymerization time. However, the grafting densities were pretty similar at different stages of the polymerization ranging from 1.13 to 1.32 chains/nm^2. The initiator densities on the nanoparticle surfaces were also estimated from the TGA results. Taking into account the fact that SiO_2 ashes remained in the residue after the burn-off of initiators, we estimated the initiator density to be 26.7 molecules/nm^2. This extremely high level of initiator density indicated that the triethoxysilane-based initiators did not form well-organized monolayers on the nanoparticle surface. Instead, a multilayer structure of initiators was formed due to the self-condensation of triethoxysilanes. Comparing the polymer grafting density to the surface initiator density, we found that the grafting efficiency was very low, about every 20 initiator moieties initiated one polymer chain. Low initiation efficiency is a common problem in surface-initiated ATRP. It is probably due to steric congestion of initiators on the nanoparticle surface, or due to the termination reactions between neighboring free radicals.

Fig. 5 shows the TEM images of pristine Ni, Ni-*g*-PMMA and Ni-*g*-PNIPAM nanoparticles cast from dilute solutions and dried under ambient conditions. As seen in Fig. 5(a), the average size of the pristine Ni nanoparticles was roughly 10 nm. The pristine Ni nanoparticles aggregated together to form big clusters. After the polymer modification, as shown in Fig. 5(b) and (c), the Ni-*g*-PMMA and Ni-*g*-PNIPAM nanoparticles were well separated without significant aggregation. The few aggregates of Ni-*g*-PNIPAM nanoparticles found in Fig. 5(c) may arise during the solvent evaporation, where the hydrophilic PNIPAM coated nanoparticles aggregated together to reduce their surface energy in the atmosphere. The TEM data further confirmed that the grafted polymers really helped to improve the dispersibility and stability of Ni nanoparticles in appropriate solvents. No appreciable change in the size of the Ni nanoparticle before and after modification was found in the TEM images. This might be because the polymer layers were difficult to be seen under TEM.

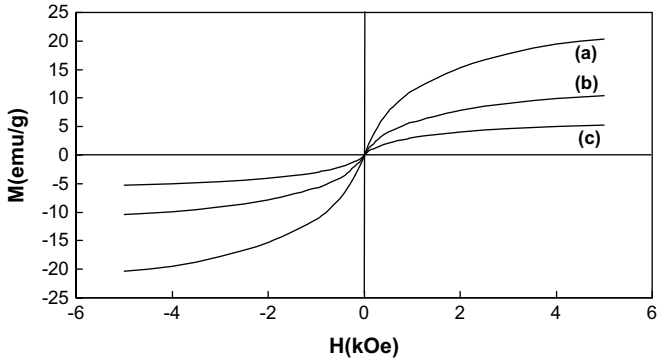

Fig. 6. Field dependant magnetization at 298 K for (a) pristine Ni nanoparticles and (b,c) PMMA coated Ni nanoparticles after polymerization time of 3 and 10 h, respectively.

The dispersibility and dispersion stability of nanoparticles are of great importance for practical applications. Before the polymer modification, the pristine Ni nanoparticle and initiator-modified Ni nanoparticle dispersions were not very stable. We can observe that the nanoparticles can slowly precipitate out from organic solvents, such as THF, DMF, methanol, etc. On the other hand, after the polymer modification, the stability of Ni nanoparticle dispersions in appropriate solvents was greatly improved. For instance, Ni-*g*-PMMA can be well dispersed in organic solvents like toluene, THF, CH_2Cl_2, etc. Ni-*g*-PNIPAM can be readily dispersed in more polar solvents like methanol, DMF and water. Even after dispersion in solvents for 6 months, no precipitation of the Ni-*g*-polymer nanoparticles was observed. From the huge difference in dispersibility and stability between the pristine Ni nanoparticles and Ni-*g*-polymer nanoparticles, we can draw the conclusion: the polymer chains were grafted from the nanoparticle surfaces. They can act as a new interface to increase the affinity between the solvent and the nanoparticles, also, they can effectively inhibit aggregation of the nanoparticles.

Nickel nanoparticle is an important type of magnetic materials. To investigate the effect of polymer coating on its magnetic properties, magnetic measurements were performed on pristine Ni nanoparticles, Ni-*g*-PMMA (3 h) and Ni-*g*-PMMA (10 h) with a superconducting quantum interference device (SQUID). Magnetic hysteresis loops above and below its blocking temperature were measured and the magnetic characteristic data are listed in Table 2. At 5 K, below the blocking temperature, all samples were ferrimagnetic, and the coercivity was about 400 Oe. The saturation magnetization value could be adjusted through control of the polymer shell thickness. For pristine Ni nanoparticle, the saturation magnetization was 32.7 emu/g. After 3 and 10 h polymerization, the magnetization value was reduced to 12.1 and 6.4 emu/g, respectively. The reduction of magnetization was due to an increased content of the non-magnetic polymers. When calibrated against the Ni mass, the saturation magnetization value was quite similar for the pristine and PMMA-grafted Ni nanoparticles, at about 32 emu/g. The magnetic hysteresis loops at 298 K were also measured. As seen in Fig. 6, no appreciable hysteresis phenomenon was observed, which indicated that both pristine Ni and Ni-*g*-PMMA nanoparticles exhibited superparamagnetic behavior. The saturation magnetization was 31.1 emu/g for the pristine Ni and 11.7, 6.2 emu/g for Ni-*g*-PMMA (3 h), Ni-*g*-PMMA (10 h), respectively, corresponding to ~31 emu/g based on the Ni mass. These values are smaller than the saturation magnetization values (50–70 emu/g) of the most widely used magnetic nanomaterials, such as Fe_3O_4 or Fe_2O_3 nanoparticles, but are still adequate for many practical applications. In this work, we also successfully grafted polystyrene, poly(*N*,*N*′-dimethylaminoethyl methacrylate) and poly(2-hydroxyethyl methacrylate) from the Ni nanoparticles, which was confirmed by FT-IR measurements.

4. Conclusions

Ni nanoparticles have been modified with triethoxysilane-containing ATRP initiators without any aggregation through the combination of ligand exchange and condensation reaction. PMMA and PNIPAM were successfully grafted from the modified Ni nanoparticles by si-ATRP technique. The iron catalyst system offered good control over the polymerization and did not impose corrosion threat to the nanoparticles. After grafted with polymers, the Ni nanoparticles possessed greatly improved dispersion and stability appropriate solvents. TEM studies confirmed that the grafted polymer formed a shell structure around the Ni nanoparticle core. The formed core–shell nanoparticles retained their magnetic properties.

This work demonstrated an effective and controllable approach to modify reactive metal nanoparticles with stable polymer shells.

Acknowledgement

We thank the Emerging Materials Knowledge (EMK) program of the Ontario Centre of Excellence (OCE) for supporting this work. We thank Dofasco Inc. for donating some of the metal samples and assistance in the corrosion analysis. We also thank the Canada Foundation of Innovation (CFI) for supporting our lab equipment and facilities.

References

[1] He YQ, Li XG, Swihart MT. Chem Mater 2005;17:1017.
[2] Sedlackova K, Czigany Z, Ujvari T, Bertoti I, Grasin R, Kovacs GJ, et al. Nanotechnology 2007;18.
[3] Chen DH, Wu SH. Chem Mater 2000;12:1354.
[4] Chen DH, Hsieh CH. J Mater Chem 2002;12:2412.
[5] Wu SH, Chen DH. Chem Lett 2004;33:406.
[6] Wojcieszak R, Zielinski M, Monteverdi S, Bettahar MM. J Colloid Interface Sci 2006;299:238.
[7] Park J, Kang E, Son SU, Park HM, Lee MK, Kim J, et al. Adv Mater 2005;17:429.
[8] Alonso F, Calvino JJ, Osante I, Yus M. Chem Lett 2005;34:1262.
[9] Han M, Liu Q, He JH, Song Y, Xu Z, Zhu JM. Adv Mater 2007;19:1096.
[10] Zhong ZY, Mastai Y, Koltypin Y, Zhao YM, Gedanken A. Chem Mater 1999;11:2350.
[11] Couto GG, Klein JJ, Schreiner WH, Mosca DH, de Oliveira AJA, Zarbin AJG. J Colloid Interface Sci 2007;311:461.
[12] Zhou L, Yuan W, Yuan J, Hong X. Mater Lett 2008;62:1372.
[13] Wu T, Zhang YF, Wang XF, Liu SY. Chem Mater 2008;20:101.
[14] Li DX, Cui Y, Wang KW, He Q, Yan XH, Li JB. Adv Funct Mater 2007;17:3134.
[15] Vestal CR, Zhang ZJ. J Am Chem Soc 2002;124:14312.
[16] Chen RX, Zhu SP, Maclaughlin S. Langmuir 2008;24:6889.
[17] Hou Y, Kondoh H, Ohta T, Gao S. Appl Surf Sci 2005;241:218.
[18] Matsuno R, Yamamoto K, Otsuka H, Takahara A. Macromolecules 2004;37:2203.
[19] Kong XX, Kawai T, Abe J, Iyoda T. Macromolecules 2001;34:1837.
[20] Ohno K, Moringa T, Koh K, Tsujii Y, Fukuda T. Macromolecules 2005;38:2137.